bioRxiv preprint doi: https://doi.org/10.1101/2021.08.23.457411; this version posted August 25, 2021. The copyright holder for this preprint (which was not certified by peer review) is the author/funder. All rights reserved. No reuse allowed without permission.

Woodsmoke particulates alter expression of antiviral host response genes in human nasal epithelial cells infected with SARS-CoV-2 in a sex-dependent manner

Woodsmoke in nasal epithelial response to SARS-CoV-2

Authors:

Stephanie A. Brocke[1], Grant T. Billings[2], Sharon Taft-Benz[3], Neil E. Alexis[4], Mark T. Heise[3,5], Ilona Jaspers[1,4]*

* Corresponding author: ilona_jaspers@med.unc.edu

116 Manning Dr. 4310 Mary Ellen Jones Bldg., Chapel Hill, NC 27599

Affiliations:

1 Curriculum in Toxicology and Environmental Medicine, University of North Carolina, Chapel Hill, NC

2 Crop and Soil Sciences Department, North Carolina State University, Raleigh, NC

3 Department of Genetics, University of North Carolina School of Medicine, Chapel Hill, NC

4 Center for Environmental Medicine, Asthma, and Lung Biology, University of North Carolina, Chapel Hill, NC

5 Department of Microbiology and Immunology, University of North Carolina, Chapel Hill, NC

Abstract:

We have previously shown that exposure to particulate air pollution, both from natural and anthropogenic sources, alters gene expression in the airways and increases susceptibility to respiratory viral infection. Additionally, we have shown that woodsmoke particulates (WSP) affect responses to influenza in a sex-dependent manner. In the present study, we used human nasal epithelial cells (hNECs) from both sexes to investigate how particulate exposure could modulate gene expression in the context of SARS-CoV-2 infection. We used diesel exhaust particulate (DEP) as well as WSP derived from eucalyptus or red oak wood. HNECs were exposed to particulates at a concentration of 22 μg/cm^2 for 2 h then immediately infected with SARS-CoV-2 at a MOI (multiplicity of infection) of 0.5. Exposure to particulates had no significant effects on viral load recovered from infected cells. Without particulate exposure, hNECs from both sexes displayed a robust upregulation of antiviral host response genes, though the response was greater in males. However, WSP exposure before infection dampened expression of genes related to the antiviral host response by 72 h post infection. Specifically, red oak WSP

bioRxiv preprint doi: https://doi.org/10.1101/2021.08.23.457411; this version posted August 25, 2021. The copyright holder for this preprint (which was not certified by peer review) is the author/funder. All rights reserved. No reuse allowed without permission.

downregulated *IFIT1*, *IFITM3*, *IFNB1*, *MX1*, *CCL3*, *CCL5*, *CXCL11*, *CXCL10*, and *DDX58*, among others. After sex stratification of these results, we found that exposure to WSP prior to SARS-CoV-2 infection downregulated anti-viral gene expression in hNECs from females more so than males. These data indicate that WSP, specifically from red oak, alter virus-induced gene expression in a sex-dependent manner and potentially suppress antiviral host defense responses following SARS-CoV-2 infection.

Author Contributions:

IJ, SAB, and MTH conceived and designed the study; SAB and STB performed experimentation and collection of data; GTB and SAB analyzed data and prepared figures; SAB, IJ, and NEA conceptualized the manuscript; SAB and IJ drafted the manuscript; SAB, NEA, and IJ provided critical revision of the manuscript and interpretation of findings; SAB, GTB, STB, NEA, MTH, and IJ approved the final version of the manuscript.

Keywords:

Woodsmoke, particulate matter (PM), sex difference, nasal epithelium, antiviral defense, SARS-CoV-2 host response

bioRxiv preprint doi: https://doi.org/10.1101/2021.08.23.457411; this version posted August 25, 2021. The copyright holder for this preprint (which was not certified by peer review) is the author/funder. All rights reserved. No reuse allowed without permission.

Introduction

Several concurrent natural disasters occurred in 2020 in the United States and abroad. Record-breaking wildfires ravaged the western United States and the COVID-19 pandemic posed a substantial public health burden around the world. Over 10 million acres of land were burned by wildfires in the United States in 2020 (1). This marked the second-highest acreage burned in a single year since the National Interagency Fire Center began recording in 1983 (1). Indeed, the area burned each year by wildfires has been trending upward in the United States for several decades (2).

Wildfires contribute significantly to air pollution and ambient particulate matter (PM). Particulate air pollution released from burning wildlands is associated with negative respiratory and cardiovascular health outcomes (reviewed in (3-6)) the toxicity of which depends heavily on the type of biomass burned and the burn temperature (7). Wildland firefighters and people who live downwind of or near to wildfires are exposed to high levels of PM released by fires (8). Studies have shown that wildland firefighters can be exposed to respirable particulate matter at concentrations >1 mg/m^3 over the course of their work shift with maximum exposures reaching >2.5 mg/m^3 (9-11). Large, populous regions of the western United States were exposed to unhealthy (>150 µg/m^3) or hazardous (>300 µg/m^3) air quality from $PM_{2.5}$ and PM_{10} during September of 2020 (Fig. 1) (12). Epidemiological studies examining the health effects of wildfires showed an association between $PM_{2.5}$ from wildfires and increased respiratory hospitalizations across 16 western states (13). A similar health effects study in California showed that women were more likely than men to visit the hospital for asthma- or hypertension-related reasons due to an increase in wildfire-generated $PM_{2.5}$ (14).

Coinciding with record-breaking wildfires is the global coronavirus disease 2019 (COVID-19) pandemic that is, to date, responsible for over 3.8 million deaths worldwide (15). Sex has been found to affect COVID-19 outcomes with males more likely than females to develop severe or fatal cases of the disease (16-18).

SARS-CoV-2, the etiologic agent behind COVID-19, primarily affects the respiratory system (19) and exhibits tropism for cells of the upper airways, with nasal epithelial cells displaying the highest susceptibility to infection compared to bronchial and lower airway epithelium (20). Primary human nasal epithelial cells (hNECs) grown *in vitro* at air-liquid interface mimic *in vivo* differentiation patterns, evidenced by expression of mucins, presence of beating cilia, and tight junction formation (21, 22). Because the nasal epithelium expresses the SARS-CoV-2 viral entry factors ACE2 and TMPRSS2 in ciliated and secretory cells (23), the differentiated hNEC model is an

bioRxiv preprint doi: https://doi.org/10.1101/2021.08.23.457411; this version posted August 25, 2021. The copyright holder for this preprint (which was not certified by peer review) is the author/funder. All rights reserved. No reuse allowed without permission.

excellent *in vitro* culture system to study SARS-CoV-2 pathogenesis. Along with biological aerosols, nasal epithelial cells are exposed to airborne particulates, gaseous pollution, and allergens. Thus, in addition to being a suitable model for studying respiratory viral infection (24, 25), hNECs demonstrate utility for toxicological studies involving aerosolized (26, 27), gaseous (28), and particulate (24) toxicants.

Exposure to air pollution is known to alter susceptibility to respiratory viral infection (reviewed in (29, 30)). *In vitro* models of respiratory epithelium treated with diesel exhaust particulate (DEP) prior to influenza infection increased viral attachment and the number of virus-infected cells relative to untreated cells (24). Rebuli and colleagues recently showed that red oak woodsmoke exposure followed by live attenuated influenza virus (LAIV) inoculation suppressed expression of host defense genes in women and upregulated many pro-inflammatory genes in men (31). Numerous epidemiological studies from around the world have found correlations between ambient air pollution levels and COVID-19 case number or case fatality rate (32-36). Recently, two studies found positive associations between ambient wildfire-derived $PM_{2.5}$ and COVID-19 cases and deaths in the western United States (37, 38).

The present study examined the interactive effects of sex, exposure to WSP, and SARS-CoV-2 infection on gene expression in hNECs. To do this we exposed hNECs derived from healthy human donors to DEP or WSP derived from burned eucalyptus or red oak. Particulate exposures occurred prior to infection with SARS-CoV-2 and sampling occurred at 0, 24, and 72 h post infection (p.i.). We assembled a panel of 46 genes related to respiratory viral infection and host immune response, including the SARS-CoV-2 entry factor (ACE2), several airway proteases, interferons and interferon-stimulated genes (ISGs), cytokines, transcription factors, pathogen recognition receptors, mucins, and surfactants. We report here that sex significantly affects hNEC transcriptional responses to SARS-CoV-2 infection and to WSP exposure. We found that males displayed a more robust upregulation of immune and antiviral genes in response to infection compared to females, but WSP exposure prior to infection significantly downregulated these genes in females with few effects in males. Together, data presented here provide a link between exposure to WSP and modification of SARS-CoV-2 induced antiviral host defense responses in the nasal mucosa.

Methods

Primary Nasal Epithelial Cell Donors

bioRxiv preprint doi: https://doi.org/10.1101/2021.08.23.457411; this version posted August 25, 2021. The copyright holder for this preprint (which was not certified by peer review) is the author/funder. All rights reserved. No reuse allowed without permission.

Collection of primary hNECs from adults was performed as previously described (22). Superficial nasal epithelial scrape biopsies were obtained from N=13 (7F, 6M) healthy, non-smoking adults with a Rhino-Pro curette (Arlington Scientific, Inc. 96-0900) per protocols approved by the University of North Carolina School of Medicine Institutional Review Board for Biomedical Research (protocol numbers 05-2528, 09-0716, 11-1363). Written informed consent was obtained from all study participants. Demographic information about the donors used for each exposure including age, BMI, and race is provided in Table 1. Nasal biopsies were stored in RPMI-1640 medium (Gibco 11875-093) on ice until further processing.

Expansion and Culture of hNECs

Culture of hNECs was performed as previously described (22, 27). Cells from nasal biopsy were expanded at passage 0 on a 12-well, PureCol-coated (Advanced Biomatrix 5005-100ML) cell culture plate (Costar 3512) in PneumaCult -Ex Plus Medium (Stemcell Technologies 05041, 05042) supplemented with hydrocortisone (Stemcell Technologies 07925), antibiotic antimycotic solution (Sigma A5955), and gentamicin reagent solution (Gibco 15750-060). Cells were passaged and further expanded in 25 cm^2 tissue culture flasks (Corning 430639) until passage 2. HNECs were then seeded on 12 mm transwell inserts with 0.4 µm pores (Costar 3460) coated with human placental collagen (Sigma C7521-10MG) at a density of 203,000-333,000 cells per well and maintained in PneumaCult -Ex Plus Medium. Once confluency was reached on the transwells, the cultures were taken to air-liquid-interface (ALI) and the apical medium was permanently removed, while the basolateral medium was switched for PneumaCult ALI Medium (Stemcell Technologies 05002, 05003, 05006), supplemented with 1% pen strep (Gibco 15140-122), hydrocortisone (Stemcell Technologies 07925), and heparin (Stemcell Technologies 07980). After this point, three times per week the basolateral medium was changed and the apical surfaces of the cultures were washed with 37°C HBSS + $CaCl_2$, + $MgCl_2$ (HBSS++) (Gibco 14025-092). Mucociliary differentiation of the cultures was achieved after 4-6 weeks of ALI conditions. At the time of exposure, cultures were at ALI for 5.29-9.14 weeks.

Diesel Exhaust Particulate (DEP) Suspension Preparation

Whole diesel exhaust particulate material from an automobile engine was collected as described by Sagai, et al. (39). Twenty-five mg of the DEP was diluted in 5 ml of warmed (37°C) phenol red-free MEM basal medium

bioRxiv preprint doi: https://doi.org/10.1101/2021.08.23.457411; this version posted August 25, 2021. The copyright holder for this preprint (which was not certified by peer review) is the author/funder. All rights reserved. No reuse allowed without permission.

(Gibco 51200-038). The suspension was sonicated with a Fisher Sonic Dismembrator Model 500 with a microprobe tip for two 1-minute cycles. During each cycle the probe was moved up and down in the suspension, and sonication alternated between 30% output for 0.5 s and 0% output for 0.5 s. After each cycle, the suspension was mixed by inversion. An additional 20 ml of warmed (37°C) medium was then added to the suspension to achieve a final concentration of 1 mg/ml. Aliquots of the suspension were snap frozen in liquid nitrogen and stored at -80°C for future use.

Woodsmoke Particulate (WSP) Suspension Preparation

Woodsmoke generated from eucalyptus and red oak were each collected as previously described by Kim, et al. (7). Briefly, eucalyptus or red oak were burned in a quartz tube furnace at 640°C and smoke was collected in a series of cryogenic traps. The resulting woodsmoke particulate condensates were then collected in acetone and concentrated with a rotary evaporator. Finally, the particulates were dried and the solid PM was resuspended in Dulbecco's PBS (Gibco 14200-075) at 2 mg/ml and frozen at -20°C. Prior to exposure, aliquots were sonicated in a water bath sonicator (Sinosonic Industrial Co. Ltd., Taiwan, Model B200) at 40 KHz for 4.75 minutes.

Particle Size Measurements of Particulate Suspensions

Particle size distributions of the three particulate suspensions were determined by diluting an aliquot of each to 50 µg/ml in ddH_2O. The diluted suspensions were run through a BD FACSVerse 2013 Flow Cytometer for size measurement and compared to size calibration standards (Thermo Fisher F13838) of 1.0, 2.0, 4.0, 6.0, 10.0, and 15.0 µm in diameter. Graphs of particle size distribution overlaid with the standard sizes are shown in Supplemental Fig. S1.

Exposure of hNECs to DEP or WSP

A pictorial depiction of the exposure and infection scheme is provided in Fig. 2. The apical surface of each culture was washed with 100 µl of warmed (37°C) HBSS++ and carefully aspirated. Basolateral medium was removed and replaced with 1.0 ml of 37°C PneumaCult ALI Medium. Warm ALI Medium was used as the control exposure and as the vehicle for particulate exposures. HNECs from three male and three female donors were used for

bioRxiv preprint doi: https://doi.org/10.1101/2021.08.23.457411; this version posted August 25, 2021. The copyright holder for this preprint (which was not certified by peer review) is the author/funder. All rights reserved. No reuse allowed without permission.

each type of exposure (DEP, eucalyptus WSP, and red oak WSP). Particulate stock aliquots were diluted in ALI medium and applied to the apical surface of the experimental wells at a concentration of 22 μg/cm^2 in 150 μl, a dose we have studied previously (24). Control wells received 150 μl ALI medium apically. Cultures were then returned to the incubator (37°C, 5% CO_2) for 2 h.

Infection with SARS-CoV-2 or Mock

At the end of the 2-h exposure, half the wells exposed to particulate and half the control wells were apically infected with SARS-CoV-2 derived from clinical isolate WA1 (20) in high glucose DMEM (Gibco 11995-065) with 5% heat-inactivated fetal bovine serum, 1% L-glutamine diluted in ALI medium at a M.O.I. (multiplicity of infection) of 0.5 in 100 μl. The other half of the cultures were mock infected with 100 μl of high glucose DMEM with 5% heat-inactivated fetal bovine serum, 5% L-glutamine diluted in ALI medium. Cultures were then returned to the incubator (37°C, 5% CO_2) for 2 h.

Sample Collection

After the 2-h infection, cells were checked under the microscope for signs of cell death. The apical liquid was carefully removed from every well. Cultures were then washed with 200 μl 37°C HBSS++ and returned to the incubator until collection. At the time of collection (0, 24, or 72 h p.i.), 100 μl 37°C HBSS++ was added to the apical surface of each culture, and cells were returned to the incubator for 15 m. Apical washes were then carefully collected and analyzed for viral titer. Cells were lysed using 350 μl cold TRIzol reagent (Life Technologies 15596018) for subsequent gene expression analysis.

Determination of Viral Titer

Fifty microliters of the apical wash were mixed with 450 μl of medium (DMEM + 5% FBS + 1% L-glutamine) followed by ten-fold serial dilutions resulting in a dilution series of 10^{-1} to 10^{-6}. Two hundred μl of each dilution was added to plated Vero E6 cells (C1008, ATCC) and incubated at 37°C. Plates were rocked every 15 min to ensure even distribution of the virus over the surface of the well. After 1 h, 2 ml of overlay (50:50 mixture of 2.5% carboxymethylcellulose and 2X alpha MEM containing 6% FBS + 2% penicillin/streptomycin + 2% L-glutamine + 2% HEPES) was added to each well. Plates were incubated at 37°C, 5% CO_2 for 4 days, then fixed with 2 ml

bioRxiv preprint doi: https://doi.org/10.1101/2021.08.23.457411; this version posted August 25, 2021. The copyright holder for this preprint (which was not certified by peer review) is the author/funder. All rights reserved. No reuse allowed without permission.

of 4% paraformaldehyde left on overnight. Following removal of the fixative, wells were rinsed with water to remove residual overlay and then stained with 0.25% crystal violet. Visible plaques were counted and averaged between two technical replicate wells. Viral titers were calculated as plaque forming units (pfu) per ml. The limit of detection for the assay was determined to be 12.5 pfu / wash, and samples that yielded no plaques were assigned a value of 6.25, half of the limit of detection.

RNA extraction from whole cell lysates in TRIzol

Whole cell lysates in TRIzol reagent were thawed on ice. An additional 650 µl cold TRIzol was added to each sample to facilitate RNA collection. Two hundred µl chloroform was added to each tube and tubes were shaken vigorously and incubated at room temperature for 3 minutes. Samples were then centrifuged for 15 minutes at 12,000 x g at 4°C. The aqueous phase containing RNA was then carefully removed from each sample and transferred to new microcentrifuge tubes. One volume of 100% ethanol was added per volume of aqueous phase removed and samples were vortexed. Samples were further processed with the Zymo RNA Clean and Concentrator Kit (Zymo R1016) according to the manufacturer's instructions. Eluted RNA was stored at -80°C until use.

Generation of cDNA and Quantification of Gene Expression of 48 genes by qPCR

RNA concentration and purity were measured using a CLARIOstar plate reader and an LVis Plate (BMG LABTECH). For each sample, 800 ng of RNA was used to generate cDNA in a reaction volume of 25 µl. The final concentrations of reagents in each reaction were as follows: 0.50 mM dNTPs (Promega U151B), 1.00 U/µl RNasin Ribonuclease Inhibitor (Promega N211A), 10.0 U/µl M-MLV Reverse Transcriptase (Invitrogen 28025-013), 0.10 µg/µl Random Primers (Invitrogen 58875), 50.0 mM KCl, 0.25 mM $MgCl_2$, 20.0 mM Tris-HCl, 0.01 mg/ml BSA. PCR was performed in 96-well plates (Thermo AB-0600, AB-0851) for one cycle (25.0°C for 10 minutes, 37.0°C for 50 minutes, 70.0°C for 15 minutes, followed by 4.0°C infinite hold). Samples were submitted to the UNC School of Medicine Center for Gastrointestinal Biology and Disease Advanced Analytics Core for high-throughput qPCR gene expression analysis. Gene expression of a panel of 48 genes (including 2 reference genes) was assayed in a Fluidigm BioMark HD system using TaqMan primers and probes. The list of primer/probe catalog numbers for all genes assayed is provided in Table 2. Duplicate Ct values were measured

bioRxiv preprint doi: https://doi.org/10.1101/2021.08.23.457411; this version posted August 25, 2021. The copyright holder for this preprint (which was not certified by peer review) is the author/funder. All rights reserved. No reuse allowed without permission.

for each sample/gene combination and averaged for further analysis. Gene expression was calculated using the ΔΔCt method with normalization to the geometric mean of expression of the two reference genes (*ACTB* and *GAPDH*). Two samples (out of 216) showing poor amplification across the panel (i.e. comparable to the no-template controls) were excluded from the data set and not further analyzed.

Quantification of SARS-CoV-2 N1 and N2 gene expression by qPCR

Expression of viral SARS-CoV-2 N1 and N2 genes was also quantified and normalized to human RNase P gene expression using the Integrated DNA Technologies 2019-nCoV RUO Kit (IDT 10006713). For a single reaction, 6.5 µl nuclease-free water, 1.5 µl of one primer/probe mix, and 10 µl of TaqMan Universal Master Mix II, with UNG (Thermo Fisher 4440038) were mixed and added to every well of a Sapphire 96-well PCR Microplate (Greiner Bio-one 652260). cDNA was then added to each well (2 µl) for a total volume of 20 µl per reaction. The plate was sealed with a plate film (Thermo Fisher 4311971) and centrifuged for 5 minutes at 500 x g at room temperature. RT-qPCR was performed on a QuantStudio 3 using the following reaction conditions: hold 50.0°C for 2 minutes then hold 95.0°C for 10 minutes, cycle through 95.0°C for 15 s and 60.0°C for 1 minute for 40 cycles. Transitions between temperatures occurred at 1.6°C/s. The two samples excluded from the Fluidigm PCR data were also excluded here. Results were collected as Ct and analyzed with the ΔΔCt method, normalized to expression of human RNase P.

Statistical Analysis

Analysis was carried out using SAS PROC MIXED as a full factorial design, with sex (M or F), particulate treatment (control, DEP, eucalyptus WSP, or red oak WSP), virus or no virus, and duration (0, 24, or 72 h), as well as all their interactions. Donor was fit as a random effect. Preplanned hypothesis tests for differences between marginal means were carried out as t-tests with the LSMESTIMATE command. Sex-specific means were calculated for each combination of particulate treatment, virus, and duration and differences were tested using a t-test with the LSMESTIMATE command. Correction for multiple comparisons was performed across all statistical tests for the entire experiment using the ‘qvalue’ R package (v. 2.22.0), with a false discovery rate q-value threshold of 0.05, assuming pi0 = 1 (equivalent to Benjamini-Hochberg correction). The resultant p-value

bioRxiv preprint doi: https://doi.org/10.1101/2021.08.23.457411; this version posted August 25, 2021. The copyright holder for this preprint (which was not certified by peer review) is the author/funder. All rights reserved. No reuse allowed without permission.

for statistical significance was $p \leq 0.00369$. Viral titer data was analyzed using GraphPad Prism v. 8.4.0. Unpaired t-tests (with Welch's correction when appropriate) were used to evaluate differences in $\log_{10}$-transformed data.

Results

Particulate exposure does not affect viral load in hNECs

Previously, we found that exposing hNECs and other airway epithelial cells to DEP prior to infection with influenza A enhanced viral replication and susceptibility to viral infection (24). In the present study, we thus sought to determine whether DEP and WSP would have similar effects in a SARS-CoV-2 infection model. HNECs were exposed to control (ALI medium) or 22 μg/cm^2 DEP, eucalyptus WSP, or red oak WSP for 2 h, followed by infection with SARS-CoV-2. Viral loads in apical washes for the hNECs exposed to particulates and their respective controls at 0, 24, and 72 h p.i. are shown in Fig. 3 A-C. The amount of infectious virus recovered from apical washes increased with duration of infection (Fig. 3 D), suggesting increased viral replication and apical secretion over time, consistent with our previous study (20). Exposure to particulates, regardless of type, had no effect on viral loads in apical washes (Fig. 3 A-C). On average, viral load recovered from males was higher than viral load recovered from hNECs from female donors, though the difference in viral loads between the sexes did not reach statistical significance (Fig. 3 D).

Expression levels for a panel of 48 genes were determined in hNECs infected with SARS-CoV-2. The relationship between the expression level of each gene (relative to reference genes) and the viral titer recovered from respective samples is shown in Fig. 4. As expected, expression levels of SARS-CoV-2 N1 and N2 genes are highly correlated with viral load recovered (Pearson's $r = 0.91$ for both). This indicates that apical release of infectious viral particles is highly correlated with viral mRNA levels. The following genes are also correlated with viral titer, with a statistically significant Pearson's $r > 0.70$: *ACE2*, *IFIT1*, *IFITM3*, *IFNB1*, *IFNL1*, *IFNL2*, *MX1*, *CCL5*, *CXCL10*, *IRF7*, *STAT1*, *DDX58*, and *TLR9*. Interestingly, *TMPRSS2* and *IL1B* both appear to be negatively correlated with viral titer.

SARS-CoV-2 infection greatly affects expression of antiviral host response genes in hNECs

In order to assess how particulate exposure affects expression of antiviral host defense genes in the presence of an infection, we first needed to measure the independent effects of SARS-CoV-2 infection on gene expression. Thus, hNECs from male and female donors which were not exposed to any particulates were

bioRxiv preprint doi: https://doi.org/10.1101/2021.08.23.457411; this version posted August 25, 2021. The copyright holder for this preprint (which was not certified by peer review) is the author/funder. All rights reserved. No reuse allowed without permission.

infected with SARS-CoV-2 (or mock infected with vehicle). At 0, 24, or 72 h p.i., cells were lysed, and RNA was extracted and purified for RT-qPCR. Gene expression in infected cultures was compared to that of corresponding uninfected cultures after normalization to reference gene expression. Virus-induced changes in gene expression in hNECs at 0, 24, and 72 h p.i. are shown in Fig. 5 and fold-inductions and p-values are tabulated in Table 3. By 24 h p.i., the Type III IFNs (*IFNL1* and *IFNL2*) were upregulated in hNECs from male and female donors, with statistically significant upregulation of both genes in males. Expression of *IFNL1* and *IFNL2* were even more highly upregulated at 72 h p.i. and reached statistical significance in both sexes. Additionally, by 72 h p.i., many other genes related to antiviral defense, cell signaling, and immune cell recruitment were significantly upregulated relative to the uninfected cells. Transcription factors, especially *IRF7* and *STAT1* were upregulated in hNECs from male and female donors at 72 h p.i., and *DDX58*, which encodes RIG-I, a cytoplasmic viral nucleic acid receptor, was also upregulated in both sexes. *ACE2* expression was significantly upregulated at 72 h p.i. in hNECs from both sexes. In most instances, gene expression in hNECs from males was more highly induced by infection than in hNECs from females, suggesting an overall more robust epithelial response to SARS-CoV-2 in hNECs from male donors. For each gene that was differentially expressed in infected cells from both sexes, the ratio of expression in males:females was calculated. Indeed, on average the level of virus-induced gene expression in hNECs from males was 2.08 times (95% CI: ± 0.57) that of hNECs from females. Additionally, we assessed whether baseline differences in gene expression existed between the sexes in uninfected cells. There were no statistically significant differences in baseline gene expression between hNECs from males and females at 24 and 72 h post mock infection (data not shown).

Particulate exposure alone has modest effects on expression of antiviral host response genes

Next, we assessed how exposure to particulates alone, without subsequent viral infection, would affect expression of our panel of antiviral host response genes. Again, hNECs from male and female donors were exposed to one of three particulates (DEP, eucalyptus WSP, or red oak WSP) or control for 2 h, followed by a "mock" infection for 2 h. Results are shown graphically in Supplemental Fig. S2 and statistically significant results are reported in Supplemental Table S1. At 0 h p.i. (mock infection), exposure to both types of WSP increased expression of *IL6* and eucalyptus WSP also upregulated expression of *IL1B*. Further, DEP and red oak WSP significantly decreased expression of *IFNG* at 0 h p.i. (data for eucalyptus WSP not shown due to missing data

bioRxiv preprint doi: https://doi.org/10.1101/2021.08.23.457411; this version posted August 25, 2021. The copyright holder for this preprint (which was not certified by peer review) is the author/funder. All rights reserved. No reuse allowed without permission.

points). By 24 h p.i. both eucalyptus WSP and red oak WSP further upregulated *IL1B* expression, while *IL6* was no longer upregulated. Overall, by 24 and 72 h p.i., particulate treatment in the absence of infection modestly affected expression of the genes in our panel in hNECs.

Woodsmoke particulates affect expression of virus-induced genes in hNECs infected with SARS-CoV-2

We hypothesized that exposure to particulates would dampen expression of crucial antiviral host response genes upon subsequent SARS-CoV-2 infection. To test this, hNECs from male and female donors were exposed to control or DEP, eucalyptus WSP, or red oak WSP for 2 h, followed by infection with SARS-CoV-2. Overall, red oak WSP caused more statistically significant changes in virus-induced gene expression than the other particulates (Table 4). DEP had very few effects on gene expression in infected cells. Further, for both types of WSP the number of statistically significant effects increased with duration of infection. More specifically, at 0 h p.i., both types of WSP increased *IL1B* and *IL6* expression compared to unexposed, infected cells, with red oak WSP exposure generating more potent upregulation of *IL6*. By 24 h p.i, all three types of particulates upregulated *IL1B* to similar degrees. At 72 h p.i. WSP exposure, especially from red oak, decreased expression of several genes, including *IFNB1*, *CCL3*, *CCL5, CXCL10*, and *CXCL11* (Fig. 6). Red oak WSP also decreased expression of *IFNL1* and *IFNL2*, albeit not statistically significantly. Other genes that are important for the antiviral response were also downregulated by eucalyptus and/or red oak, such as *IFIT1*, *IFITM3*, *MX1*, *IRF7*, *STAT1*, *STAT2*, *DDX58*, and *MMP7*. Thus, exposure to WSP prior to infection with SARS-CoV-2 suppressed IFN-dependent immune gene expression.

Woodsmoke particulate effects on gene expression in infected hNECs are sex-specific

Because the virus-induced effects on gene expression were sex-dependent (Fig. 5), we next assessed whether gene expression changes in cells exposed to particulates prior to virus infection were also sex-dependent. Few sex-specific changes were observed at 0 and 24 h p.i. (Table 5), however at 72 h p.i., WSP, especially red oak, modified virus-induced gene expression in hNECs from female donors (Fig. 7). At this timepoint, WSP from red oak caused statistically significant downregulation of *IFIT1*, *IFITM3*, *IFNB1*, *IRF7*, *STAT1*, *DDX58*, *CXCL10*, and *CXCL11*. *IFNL1* and *IFNL2* were also downregulated by red oak WSP in hNECs from females but statistical significance was not reached. Additionally, red oak WSP caused a statistically

bioRxiv preprint doi: https://doi.org/10.1101/2021.08.23.457411; this version posted August 25, 2021. The copyright holder for this preprint (which was not certified by peer review) is the author/funder. All rights reserved. No reuse allowed without permission.

significant decline in *MX1* expression in hNECs from females versus males. Eucalyptus WSP also caused sex-dependent downregulation of several genes in female donors, though the effects were more modest. These results suggest that WSP exposure, especially from red oak, greatly dampens expression of antiviral genes in hNECs from females during SARS-CoV-2 infection, with more modest effects seen in hNECS from males.

Discussion

During 2020, air quality reached unhealthy and hazardous levels in the western United States due to wildfires which coincided with the spread of COVID-19. Epidemiological evidence has shown that worsened air quality from $PM_{2.5}$ is associated with increased COVID-19 case rate and case fatality rate around the world. Additionally, toxicological studies have shown that PM treatment affects the host defense response of the airways upon viral infection. In the present study, we hypothesized that exposing hNECs to PM derived from diesel exhaust and woodsmoke, simulating wildfires, would alter the expression of host antiviral response genes upon subsequent infection with SARS-CoV-2. We also hypothesized that these effects would be sex-dependent. We found that exposure to WSP derived from red oak significantly affected gene expression in the context of SARS-CoV-2 infection, leading to downregulation of critical genes involved in host defense. These effects were more pronounced in hNECs from females, both by magnitude of effect and number of affected genes. WSP derived from eucalyptus showed a similar trend but with more modest effects while DEP exposure had little effect on gene expression during SARS-CoV-2 infection. We also found that SARS-CoV-2 infection alone altered gene expression patterns differently in hNECs from males and females, with cells from males initiating a more robust upregulation of host defense genes in response to infection. Together, these data support the notion that inhalation of wildfire smoke could adversely affect the host antiviral response to SARS-CoV-2 infection.

Our data indicate that SARS-CoV-2 induced gene expression changes in hNECs are sex-dependent, alone and in the context of WSP exposure. In response to infection, expression of many of the genes in our panel increased, matching previously reported findings about the cellular responses to SARS-CoV-2 infection. For example, induction of type I and type III interferons is well-documented in the epithelial cell response to SARS-CoV-2 infection ((40, 41) reviewed in (42, 43)). We observed significant upregulation of *IFNB1*, *IFNL1*, and *IFNL2* by 72 h p.i., while *IFNA1* and *IFNA2* were not induced. Accordingly, several interferon-stimulated genes ((44), and reviewed in (45)), regulatory factors, and related transcription factors were also induced in infected hNECs

bioRxiv preprint doi: https://doi.org/10.1101/2021.08.23.457411; this version posted August 25, 2021. The copyright holder for this preprint (which was not certified by peer review) is the author/funder. All rights reserved. No reuse allowed without permission.

from one or both sexes, such as *ACE2*, *IFIT1*, *IFITM3*, *MX1*, *DDX58*, *IRF1*, *IRF7*, *STAT1*, and *STAT2*. In addition to activating the interferon response pathway, SARS-CoV-2 is known to activate NF-κB transcription factors and result in upregulation of cytokines and chemokines to recruit immune cells, such as *CSF2*, *IL6*, *IL1B*, *TNF*, *CXCL8*, *CXCL9*, *CXCL10*, *CXCL11*, *CCL2*, *CCL3*, and *CCL5* (41, 46, 47) and reviewed in (48-51). While in our model SARS-CoV-2 infection induced expression of many of these cytokines in both sexes, by 72 h p.i. hNECs from males displayed upregulation of antiviral and immune signaling gene expression which was two times greater than gene induction in hNECs from females, on average. In contrast, in our previous study examining nasal mucosal immune responses to inoculation with live attenuated influenza virus (LAIV) vaccine, Rebuli, et al. observed a more robust antiviral and inflammatory response in female subjects exposed to LAIV compared to male subjects (31). In that study, it was hypothesized that the seemingly larger upregulation of genes involved with antiviral defense and immune cell recruitment in females could reflect differential baseline gene expression levels between the sexes (31). However, in the data presented here, no differences in baseline gene expression between the sexes were observed at 24 and 72 h p.i. This previous *in vivo* human study also revealed that exposure to woodsmoke (500 μg/m^3) for 2 h prior to inoculation with LAIV resulted in upregulation of inflammatory gene expression in males and suppression of antiviral defense genes in females (31). The data presented here showed a similar, sex-dependent response to woodsmoke exposure in the context of infection. Downregulation of genes involved in the interferon response pathway was more frequent and greater in magnitude in hNECs from females versus males treated with WSP before SARS-CoV-2 infection. Signaling molecules involved in recruitment of immune cells were also generally more downregulated in hNECs from females compared to males. These findings suggest that WSP exposure may dampen antiviral responses in females. Risk assessment studies have found that women more than men are exposed to high levels of PM from burning biomass in indoor settings, especially in developing countries (52-54). However, the opposite is true for exposure to wildfire smoke in firefighters, who are predominantly male. Furthermore, since many of the genes assayed in this study are involved in general antiviral host defense, these results may translate to other viral pathogens of public health importance and additional studies examining sex-based differences in epithelial responses to respiratory viruses alone or in the context of ambient pollutant exposures are needed.

While exposure to WSP significantly modified SARS-CoV-2 induced antiviral host gene expression, the exposures alone in the absence of infection had only modest effects. Exposing hNECs to WSP had few effects

bioRxiv preprint doi: https://doi.org/10.1101/2021.08.23.457411; this version posted August 25, 2021. The copyright holder for this preprint (which was not certified by peer review) is the author/funder. All rights reserved. No reuse allowed without permission.

on the expression of genes in our panel, besides upregulation of pro-inflammatory *IL6* and *IL1B* and downregulation of *IFNG.* This was not surprising, however, because *in vitro* studies with epithelial cells and *in vivo* human studies have provided inconclusive evidence about the effects of WSP exposure on the airways in the absence of a secondary stimulus. Some studies of human volunteers exposed to WSP did not show significant pro-inflammatory changes in the airway (55-57) while others found signs of pulmonary or systemic inflammation post WSP exposure (11, 58). Pro-inflammatory effects of WSP on epithelial cells *in vitro* are mild and inconsistent (59-61). These discrepancies could be due in part to differences in fuel types and burn conditions across studies. Kim, et al. reported that both burn fuel and temperature affected chemical composition and thus toxicity of WSP in an *in vivo* mouse exposure (7). In our study, WSP from eucalyptus and red oak demonstrated differential effects on gene expression in hNECs. WSP derived from burning red oak contains higher mass fractions of N-alkanes, inorganic and ionic species compared to WSP from eucalyptus (7). Recent data indicate that N-alkanes in PM exposures were significantly associated with inflammation (62), which is consistent with our observations. Additionally, eucalyptus WSP contain a higher mass fraction of methoxyphenols than red oak WSP, which were negatively correlated to biological response in a separate study (7, 63). Hence, the differences in chemical composition and particle size distribution (Supplemental Fig. S1) could be responsible for the differential effects of WSP from red oak and eucalyptus on hNECs.

Even though our data did not show significant differences in viral titers based on sex or particulate exposure, gene expression correlated significantly with viral titers and uncovered positive and negative associations with immune and inflammatory genes. As expected, correlation between viral titer and expression of SARS-CoV-2 N1 and N2 genes was high, indicating viral replication was contributing to viral load, which increased with duration of infection. In addition, expression levels of several IFNs (*IFNB1*, *IFNL1*, *IFNL2*) and ISGs (*IFIT1*, *IFITM3*, *ACE2*, *MX1*, *STAT1*, *DDX58*, *CXCL10*, etc.) were positively correlated with viral titer, which has been previously reported (40, 41). In contrast, *TMPRSS2* expression was negatively correlated with viral titer, which was also shown by Lieberman, et al. (41). Interestingly, *IL1B* expression was negatively correlated with viral titer in our model, and expression of *IL6*, *TNF*, and *CXCL8* showed weak positive or no associations with viral titer (*r* of 0.42, 0.14, and 0.28 respectively). These findings may be indicative of viral evasion of pro-inflammatory cytokine induction. Of the genes encoding surfactant proteins, *SFTPA1* was much more strongly associated with viral titer than *SFTPD* (*r* of 0.69 compared to 0.32), although the proteins encoded by both genes contribute to

bioRxiv preprint doi: https://doi.org/10.1101/2021.08.23.457411; this version posted August 25, 2021. The copyright holder for this preprint (which was not certified by peer review) is the author/funder. All rights reserved. No reuse allowed without permission.

the host immune response (reviewed by (64)). Similarly, *MUC5AC* was more strongly associated with viral titer than its counterpart *MUC5B* (*r* of 0.53 compared to 0.17). Expression of viral and interferon-related genes was highly correlated with viral titer, however inflammatory gene expression generally showed weak or no association with titer. These data indicate that the gene expression response to SARS-CoV-2 infection in our nasal epithelial model is dominated by the IFN response.

The fact that there were no differences in viral load recovered from exposed and unexposed hNECs, even at 72 h p.i., points at some potential limitations of the data presented here. The first is that the changes observed in gene expression at the transcript level may not translate into functional differences at the tissue level. Although *IFIT1*, *IFITM3*, *IFNB1, IFNL1*, *IFNL2*, *MX1*, *CXCL10*, *DDX58*, and other crucial genes for the antiviral response were all downregulated by particulate treatments (in hNECs from females), further investigation is necessary to determine whether these changes result in host defense decrements *in vivo*. Previously, we found agreement between transcript and protein level changes in gene expression after red oak woodsmoke exposure and LAIV inoculation in men and women (31). Further, while the respiratory epithelium represents the first line of defense to inhaled pollution and pathogens, clearance of infection and inhaled debris relies heavily upon recruitment and activation of immune cells. In our study, particulate treatment prior to infection decreased expression of several important chemokines by 72 h p.i. (Fig. 6). It is possible that *in vivo*, the WSP-induced reduction in expression of *CCL3*, *CCL5*, *CXCL10*, *CXCL11*, *CXCL9*, *IL6*, and *TNF*, all of which are chemoattractants for innate and adaptive immune cells, would result in a more widespread and lasting infection. *In vivo* exposures of mice to diesel exhaust prior to respiratory viral infection increased viral titers or viral mRNA collected from whole lungs (65, 66). Management of viral load mediated by immune cells is not captured in our monoculture model. Finally, many groups have reported effective evasion of interferon and NF-κB pathway activation by SARS-CoV-2 (67-70). Indeed, only a small fraction of infected epithelial cells express the majority of interferons and ISGs (40). This suggests that the virus successfully evades or inhibits antiviral responses in the majority of cells it infects. Additionally, Fig. 3 and Fig. 5 suggest that viral replication and release was underway by 24 h p.i., though ISGs and pro-inflammatory responses were not yet induced. The kinetic delay in cellular responses relative to viral replication as well as antiviral evasion by SARS-CoV-2 likely significantly influence the effects of co-exposure to inhaled pollutant on host responses.

bioRxiv preprint doi: https://doi.org/10.1101/2021.08.23.457411; this version posted August 25, 2021. The copyright holder for this preprint (which was not certified by peer review) is the author/funder. All rights reserved. No reuse allowed without permission.

Further work is necessary to elucidate the effects of WSP exposure on SARS-CoV-2 infection, especially in other airway cell types and with varied or mixed fuel sources. Exposure to red oak WSP prior to SARS-CoV-2 infection dampens expression of antiviral and host defense genes in nasal epithelial cells. These effects are sex-dependent, with overall greater downregulation of genes in females than in males. Men have been found to be more susceptible to severe and fatal cases of COVID-19 (18). It is possible that wildfire-derived PM could increase COVID-19 morbidity in exposed females, but additional epidemiological studies are needed. The impact of wildfire smoke on public health in the United States and abroad is expected to increase as wildfire seasons become more intense and the population exposed to wildfire smoke continues to rise (4). As viral pandemics and wildfire exposures continue to be concurrent respiratory health risks, it is important to understand the impacts air pollution from wildfires has on host defense responses so strategies for mitigating risk can be employed, especially for subpopulations already susceptible to respiratory infections.

Code Availability

SAS and R codes used for data processing, statistical analysis, and data visualization are provided as a Supplemental File.

Acknowledgments

The authors would like to acknowledge and thank the study coordinators Noelle Knight, Carole Robinette, and Martha Almond for recruiting hNEC donors and retrieving scrape biopsies. The authors would like to thank Shaun McCullough for his generous donation of DEP and Eva Vitucci for her help in making the DEP preparation and determining particulate sizes. The authors would also like to thank Yong Ho Kim and Ian Gilmour for their generous contribution of WSP samples. Finally, the authors thank the Advanced Analytics Core for their help and contributions.

Grants

Funding was provided by NIH grants R01 ES031173, T32 ES007126, and P30 DK034987.

Disclosures

The authors have no conflicts of interest to disclose.

bioRxiv preprint doi: https://doi.org/10.1101/2021.08.23.457411; this version posted August 25, 2021. The copyright holder for this preprint (which was not certified by peer review) is the author/funder. All rights reserved. No reuse allowed without permission.

References

1. **National Interagency Fire Center**. Wildfires and Acres: Total Wildland Fires and Acres (1983-2020) [Online]. https://www.nifc.gov/fire-information/statistics/wildfires. [June 14, 2021].
2. **USEPA**. Climate Change Indicators: Wildfires [Online]. https://www.epa.gov/climate-indicators/climate-change-indicators-wildfires. [June 14, 2021].
3. **Reid CE, Brauer M, Johnston FH, Jerrett M, Balmes JR, and Elliott CT**. Critical Review of Health Impacts of Wildfire Smoke Exposure. *Environmental Health Perspectives* 124: 1334-1343, 2016.
4. **Reid CE, and Maestas MM**. Wildfire smoke exposure under climate change. *Current Opinion in Pulmonary Medicine* 25: 179-187, 2019.
5. **Fann N, Alman B, Broome RA, Morgan GG, Johnston FH, Pouliot G, and Rappold AG**. The health impacts and economic value of wildland fire episodes in the U.S.: 2008-2012. *Sci Total Environ* 610-611: 802-809, 2018.
6. **Liu JC, Pereira G, Uhl SA, Bravo MA, and Bell ML**. A systematic review of the physical health impacts from non-occupational exposure to wildfire smoke. *Environmental Research* 136: 120-132, 2015.
7. **Kim YH, Warren SH, Krantz QT, King C, Jaskot R, Preston WT, George BJ, Hays MD, Landis MS, Higuchi M, Demarini DM, and Gilmour MI**. Mutagenicity and Lung Toxicity of Smoldering vs. Flaming Emissions from Various Biomass Fuels: Implications for Health Effects from Wildland Fires. *Environmental Health Perspectives* 126: 017011, 2018.
8. **Navarro K, Vaidyanathan, A**. Understanding Smoke Exposure in Communities and Fire Camps Affected by Wildfires ---- California and Oregon, 2020 Morbidity and Mortality Weekly Report: CDC, 2020.
9. **Reinhardt T, Ottmar, RD**. Baseline Measurements of Smoke Exposure Among Wildland Firefighters. *Journal of Occupational and Environmental Hygiene* 1: 593-606, 2004.
10. **Reinhardt T, Ottmar, RD**. Smoke Exposure at Western wildfires. *Pacific Northwest Research Station* Res. Pap. PNW-RP-525: 72, 2000.
11. **Swiston JR, Davidson W, Attridge S, Li GT, Brauer M, and Van Eeden SF**. Wood smoke exposure induces a pulmonary and systemic inflammatory response in firefighters. *European Respiratory Journal* 32: 129-138, 2008.
12. **United States, AIRNOW Program**. *AIRNow* [Online]. US Environmental Protection Agency, Office of Air Quality Planning and Standards,. http://www.airnow.gov/. [June, 2021].
13. **Liu JC, Wilson A, Mickley LJ, Dominici F, Ebisu K, Wang Y, Sulprizio MP, Peng RD, Yue X, Son J-Y, Anderson GB, and Bell ML**. Wildfire-specific Fine Particulate Matter and Risk of Hospital Admissions in Urban and Rural Counties. *Epidemiology* 28: 77-85, 2017.
14. **Reid C, Jerrett, M, Tager, IB, Petersen, ML, Mann, JK, Balmes, JR**. Differential respiratory health effects from the 2008 northern California wildfires: A spatiotemporal approach. *Environmental Research* 150: 227-235, 2016.
15. **World Health Organization**. WHO Coronavirus (COVID-19) Dashboard [Online]. World Health Organization. https://covid19.who.int/. [June 16, 2021].
16. **Finelli L, Gupta V, Petigara T, Yu K, Bauer KA, and Puzniak LA**. Mortality Among US Patients Hospitalized With SARS-CoV-2 Infection in 2020. *JAMA Netw Open* 4: e216556, 2021.
17. **Jin JM, Bai P, He W, Wu F, Liu XF, Han DM, Liu S, and Yang JK**. Gender Differences in Patients With COVID-19: Focus on Severity and Mortality. *Front Public Health* 8: 152, 2020.
18. **Gomez JMD, Du-Fay-De-Lavallaz JM, Fugar S, Sarau A, Simmons JA, Clark B, Sanghani RM, Aggarwal NT, Williams KA, Doukky R, and Volgman AS**. Sex Differences in COVID-19 Hospitalization and Mortality. *Journal of Women's Health* 30: 646-653, 2021.
19. **Centers for Disease Control and Prevention**. Symptoms of COVID-19 [Online]. US Dept of Health and Human Services. https://www.cdc.gov/coronavirus/2019-ncov/symptoms-testing/symptoms.html. [June, 18, 2021].
20. **Hou YJ, Okuda K, Edwards CE, Martinez DR, Asakura T, Dinnon KH, 3rd, Kato T, Lee RE, Yount BL, Mascenik TM, Chen G, Olivier KN, Ghio A, Tse LV, Leist SR, Gralinski LE, Schäfer A, Dang H, Gilmore R, Nakano S, Sun L, Fulcher ML, Livraghi-Butrico A, Nicely NI, Cameron M, Cameron C, Kelvin DJ, de Silva A, Margolis DM, Markmann A, Bartelt L, Zumwalt R, Martinez FJ, Salvatore SP, Borczuk A, Tata PR, Sontake V, Kimple A, Jaspers I, O'Neal WK, Randell SH, Boucher RC, and Baric RS**. SARS-CoV-2 Reverse Genetics Reveals a Variable Infection Gradient in the Respiratory Tract. *Cell* 182: 429-446.e414, 2020.
21. **Lee MK, Yoo JW, Lin H, Kim YS, Kim DD, Choi YM, Park SK, Lee CH, and Roh HJ**. Air-liquid interface culture of serially passaged human nasal epithelial cell monolayer for in vitro drug transport studies. *Drug Deliv* 12: 305-311, 2005.

bioRxiv preprint doi: https://doi.org/10.1101/2021.08.23.457411; this version posted August 25, 2021. The copyright holder for this preprint (which was not certified by peer review) is the author/funder. All rights reserved. No reuse allowed without permission.

22. **Müller L, Brighton LE, Carson JL, Fischer WA, and Jaspers I**. Culturing of Human Nasal Epithelial Cells at the Air Liquid Interface. *Journal of Visualized Experiments* 2013.
23. **Sungnak W, Huang N, Bécavin C, Berg M, Queen R, Litvinukova M, Talavera-López C, Maatz H, Reichart D, Sampaziotis F, Worlock KB, Yoshida M, and Barnes JL**. SARS-CoV-2 entry factors are highly expressed in nasal epithelial cells together with innate immune genes. *Nature Medicine* 26: 681-687, 2020.
24. **Jaspers I, Ciencewicki, JM, Zhang, W, Brighton, LE, Carson, JL, Beck, MA, Madden, MC**. Diesel Exhaust enhances influenza virus infections in respiratory epithelial cells. *Toxicological Sciences* 85: 990-1002, 2005.
25. **Spannhake EW, Reddy SP, Jacoby DB, Yu XY, Saatian B, and Tian J**. Synergism between rhinovirus infection and oxidant pollutant exposure enhances airway epithelial cell cytokine production. *Environ Health Perspect* 110: 665-670, 2002.
26. **Clapp PW, Lavrich KS, Van Heusden CA, Lazarowski ER, Carson JL, and Jaspers I**. Cinnamaldehyde in flavored e-cigarette liquids temporarily suppresses bronchial epithelial cell ciliary motility by dysregulation of mitochondrial function. *American Journal of Physiology-Lung Cellular and Molecular Physiology* 316: L470-L486, 2019.
27. **Escobar Y-NH, Morrison CB, Chen Y, Hickman E, Love CA, Rebuli ME, Surratt JD, Ehre C, and Jaspers I**. Differential responses to e-cig generated aerosols from humectants and different forms of nicotine in epithelial cells from non-smokers and smokers. *American Journal of Physiology-Lung Cellular and Molecular Physiology* 0: null.
28. **Kesic MJ, Meyer M, Bauer R, and Jaspers I**. Exposure to ozone modulates human airway protease/antiprotease balance contributing to increased influenza A infection. *PLoS One* 7: e35108, 2012.
29. **Ciencewicki J, and Jaspers I**. Air pollution and respiratory viral infection. *Inhal Toxicol* 19: 1135-1146, 2007.
30. **Rebuli ME, Brocke SA, and Jaspers I**. Impact of Inhaled Pollutants on Response to Viral Infection in Controlled Exposures. *Journal of Allergy and Clinical Immunology* 2021.
31. **Rebuli ME, Speen AM, Martin EM, Addo KA, Pawlak EA, Glista-Baker E, Robinette C, Zhou H, Noah TL, and Jaspers I**. Wood Smoke Exposure Alters Human Inflammatory Responses to Viral Infection in a Sex-Specific Manner. A Randomized, Placebo-controlled Study. *American Journal of Respiratory and Critical Care Medicine* 199: 996-1007, 2019.
32. **Wu X, Nethery RC, Sabath MB, Braun D, and Dominici F**. Air pollution and COVID-19 mortality in the United States: Strengths and limitations of an ecological regression analysis. *Science Advances* 6: eabd4049, 2020.
33. **Travaglio M, Yu Y, Popovic R, Selley L, Leal NS, and Martins LM**. Links between air pollution and COVID-19 in England. *Environmental Pollution* 268: 115859, 2021.
34. **Liang D, Shi L, Zhao J, Liu P, Sarnat JA, Gao S, Schwartz J, Liu Y, Ebelt ST, Scovronick N, and Chang HH**. Urban Air Pollution May Enhance COVID-19 Case-Fatality and Mortality Rates in the United States. *The Innovation* 1: 100047, 2020.
35. **Stieb DM, Evans GJ, To TM, Brook JR, and Burnett RT**. An ecological analysis of long-term exposure to PM2.5 and incidence of COVID-19 in Canadian health regions. *Environmental Research* 191: 110052, 2020.
36. **Cole M, Ozgen, C, Strobl, E**. Air Pollution Exposure and COVID-19. *IZA Institute of Labor Economics* DP No. 13367: 2020.
37. **Zhou X, Josey K, Kamareddine L, Caine MC, Liu T, Mickley LJ, Cooper M, and Dominici F**. Excess of COVID-19 cases and deaths due to fine particulate matter exposure during the 2020 wildfires in the United States. *Science Advances* 7: eabi8789, 2021.
38. **Kiser D, Elhanan G, Metcalf WJ, Schnieder B, and Grzymski JJ**. SARS-CoV-2 test positivity rate in Reno, Nevada: association with PM2.5 during the 2020 wildfire smoke events in the western United States. *Journal of Exposure Science & Environmental Epidemiology* 2021.
39. **Sagai M, Saito, H., Ichinose, T., Kodama, M., Mori, Y.** Biological Effects of Diesel Exhaust Particles. I. In Vitro Production of Superoxide and In Vivo Toxicity in Mouse. *Free Radical Biology and Medicine* 14: 37-47, 1993.
40. **Fiege JK, Thiede JM, Nanda HA, Matchett WE, Moore PJ, Montanari NR, Thielen BK, Daniel J, Stanley E, Hunter RC, Menachery VD, Shen SS, Bold TD, and Langlois RA**. Single cell resolution of SARS-CoV-2 tropism, antiviral responses, and susceptibility to therapies in primary human airway epithelium. *PLOS Pathogens* 17: e1009292, 2021.
41. **Lieberman NAP, Peddu V, Xie H, Shrestha L, Huang M-L, Mears MC, Cajimat MN, Bente DA, Shi P-Y, Bovier F, Roychoudhury P, Jerome KR, Moscona A, Porotto M, and Greninger AL**. In vivo antiviral host transcriptional response to SARS-CoV-2 by viral load, sex, and age. *PLOS Biology* 18: e3000849, 2020.
42. **Kim Y-M, and Shin E-C**. Type I and III interferon responses in SARS-CoV-2 infection. *Experimental & Molecular Medicine* 53: 750-760, 2021.
43. **Park A, and Iwasaki A**. Type I and Type III Interferons – Induction, Signaling, Evasion, and Application to Combat COVID-19. *Cell Host & Microbe* 27: 870-878, 2020.

bioRxiv preprint doi: https://doi.org/10.1101/2021.08.23.457411; this version posted August 25, 2021. The copyright holder for this preprint (which was not certified by peer review) is the author/funder. All rights reserved. No reuse allowed without permission.

44. **Ziegler CGK, Allon SJ, Nyquist SK, Mbano IM, Miao VN, Tzouanas CN, Cao Y, Yousif AS, Bals J, Hauser BM, Feldman J, Muus C, Wadsworth MH, 2nd, Kazer SW, Hughes TK, Doran B, Gatter GJ, Vukovic M, Taliaferro F, Mead BE, Guo Z, Wang JP, Gras D, Plaisant M, Ansari M, Angelidis I, Adler H, Sucre JMS, Taylor CJ, Lin B, Waghray A, Mitsialis V, Dwyer DF, Buchheit KM, Boyce JA, Barrett NA, Laidlaw TM, Carroll SL, Colonna L, Tkachev V, Peterson CW, Yu A, Zheng HB, Gideon HP, Winchell CG, Lin PL, Bingle CD, Snapper SB, Kropski JA, Theis FJ, Schiller HB, Zaragosi LE, Barbry P, Leslie A, Kiem HP, Flynn JL, Fortune SM, Berger B, Finberg RW, Kean LS, Garber M, Schmidt AG, Lingwood D, Shalek AK, and Ordovas-Montanes J**. SARS-CoV-2 Receptor ACE2 Is an Interferon-Stimulated Gene in Human Airway Epithelial Cells and Is Detected in Specific Cell Subsets across Tissues. *Cell* 181: 1016-1035.e1019, 2020.

45. **Schoggins J, Rice, CM**. Interferon-stimulated genes and their antiviral effector functions. *Curr Opin Virol* 1: 519-525, 2011.

46. **Patra T, Meyer K, Geerling L, Isbell TS, Hoft DF, Brien J, Pinto AK, Ray RB, and Ray R**. SARS-CoV-2 spike protein promotes IL-6 trans-signaling by activation of angiotensin II receptor signaling in epithelial cells. *PLOS Pathogens* 16: e1009128, 2020.

47. **Schroeder S, Pott F, Niemeyer D, Veith T, Richter A, Muth D, Goffinet C, Müller MA, and Drosten C**. Interferon antagonism by SARS-CoV-2: a functional study using reverse genetics. *The Lancet Microbe* 2: e210-e218, 2021.

48. **Hemmat N, Asadzadeh Z, Ahangar NK, Alemohammad H, Najafzadeh B, Derakhshani A, Baghbanzadeh A, Baghi HB, Javadrashid D, Najafi S, Ar Gouilh M, and Baradaran B**. The roles of signaling pathways in SARS-CoV-2 infection; lessons learned from SARS-CoV and MERS-CoV. *Archives of Virology* 166: 675-696, 2021.

49. **Hirano T, and Murakami M**. COVID-19: A New Virus, but a Familiar Receptor and Cytokine Release Syndrome. *Immunity* 52: 731-733, 2020.

50. **Hariharan A, Hakeem AR, Radhakrishnan S, Reddy MS, and Rela M**. The Role and Therapeutic Potential of NF-kappa-B Pathway in Severe COVID-19 Patients. *Inflammopharmacology* 29: 91-100, 2021.

51. **Majumdar S, and Murphy PM**. Chemokine Regulation During Epidemic Coronavirus Infection. *Front Pharmacol* 11: 600369-600369, 2021.

52. **Bede-Ojimadu O, and Orisakwe OE**. Exposure to Wood Smoke and Associated Health Effects in Sub-Saharan Africa: A Systematic Review. *Annals of Global Health* 86: 2020.

53. **Okello G, Devereux G, and Semple S**. Women and girls in resource poor countries experience much greater exposure to household air pollutants than men: Results from Uganda and Ethiopia. *Environment International* 119: 429-437, 2018.

54. **Balakrishnan K, Sambandam S, Ramaswamy P, Mehta S, and Smith KR**. Exposure assessment for respirable particulates associated with household fuel use in rural districts of Andhra Pradesh, India. *J Expo Anal Environ Epidemiol* 14 Suppl 1: S14-25, 2004.

55. **Muala A, Rankin G, Sehlstedt M, Unosson J, Bosson JA, Behndig A, Pourazar J, Nyström R, Pettersson E, Bergvall C, Westerholm R, Jalava PI, Happo MS, Uski O, Hirvonen M-R, Kelly FJ, Mudway IS, Blomberg A, Boman C, and Sandström T**. Acute exposure to wood smoke from incomplete combustion - indications of cytotoxicity. *Particle and Fibre Toxicology* 12: 2015.

56. **Sehlstedt M, Dove R, Boman C, Pagels J, Swietlicki E, Löndahl J, Westerholm R, Bosson J, Barath S, Behndig AF, Pourazar J, Sandström T, Mudway IS, and Blomberg A**. Antioxidant airway responses following experimental exposure to wood smoke in man. *Particle and Fibre Toxicology* 7: 21, 2010.

57. **Stockfelt L, Sallsten G, Almerud P, Basu S, and Barregard L**. Short-term chamber exposure to low doses of two kinds of wood smoke does not induce systemic inflammation, coagulation or oxidative stress in healthy humans. *Inhalation Toxicology* 25: 417-425, 2013.

58. **Hansson A, Rankin G, Uski O, Sehlstedt M, Bosson J, Pourazar J, Boman C, Lindgren R, Garcia Lopez N, Behndig A, Blomberg A, Sandström T, and Muala A**. Wood smoke effects on epithelial cell lines and human airway cells. *European Respiratory Journal* 54: PA5448, 2019.

59. **Dilger M, Orasche J, Zimmermann R, Paur H-R, Diabaté S, and Weiss C**. Toxicity of wood smoke particles in human A549 lung epithelial cells: the role of PAHs, soot and zinc. *Archives of Toxicology* 90: 3029-3044, 2016.

60. **Danielsen PH, Møller P, Jensen KA, Sharma AK, Wallin HK, Bossi R, Autrup H, Mølhave L, Ravanat J-L, Briedé JJ, De Kok TM, and Loft S**. Oxidative Stress, DNA Damage, and Inflammation Induced by Ambient Air and Wood Smoke Particulate Matter in Human A549 and THP-1 Cell Lines. *Chemical Research in Toxicology* 24: 168-184, 2011.

61. **Roscioli E, Hamon R, Lester SE, Jersmann HPA, Reynolds PN, and Hodge S**. Airway epithelial cells exposed to wildfire smoke extract exhibit dysregulated autophagy and barrier dysfunction consistent with COPD. *Respiratory Research* 19: 2018.

bioRxiv preprint doi: https://doi.org/10.1101/2021.08.23.457411; this version posted August 25, 2021. The copyright holder for this preprint (which was not certified by peer review) is the author/funder. All rights reserved. No reuse allowed without permission.

62. **Park J, Lee K-H, Kim H, Woo J, Heo J, Lee C-H, Yi S-M, and Yoo C-G**. The impact of organic extracts of seasonal PM2.5 on primary human lung epithelial cells and their chemical characterization. *Environmental Science and Pollution Research* 2021.

63. **Rager J, Clark, J, Eaves, LA, Avula, V, Niehoff, NM, Kim, YH, Jaspers, I, Gilmour, MI**. Mixtures modeling identifies chemical inducers versus repressors of toxicity associated with wildfire smoke. *Sci Total Environ* 775: 2021.

64. **Han S, and Mallampalli RK**. The Role of Surfactant in Lung Disease and Host Defense against Pulmonary Infections. *Ann Am Thorac Soc* 12: 765-774, 2015.

65. **Harrod K, Jaramillo, RJ, Rosenberger, CL, Wang, SZ, Berger, JA, McDonald, JD, Reed, MD**. Increased susceptibility to RSV infection by exposure to inhaled diesel engine emissions. *Am J Respir Cell Mol Biol* 28: 451-463, 2003.

66. **Gowdy K, Krantz, QT, King, C, Boykin E, Jaspers, I, Linak, WP, Gilmour, MI**. Role of oxidative stress on diesel-enhanced influenza infection in mice. *Particle and Fibre Toxicology* 7: 1-15, 2010.

67. **Xia H, Cao Z, Xie X, Zhang X, Chen JY-C, Wang H, Menachery VD, Rajsbaum R, and Shi P-Y**. Evasion of Type I Interferon by SARS-CoV-2. *Cell reports* 33: 108234-108234, 2020.

68. **Lei X, Dong X, Ma R, Wang W, Xiao X, Tian Z, Wang C, Wang Y, Li L, Ren L, Guo F, Zhao Z, Zhou Z, Xiang Z, and Wang J**. Activation and evasion of type I interferon responses by SARS-CoV-2. *Nature Communications* 11: 3810, 2020.

69. **Hayn M, Hirschenberger M, Koepke L, Nchioua R, Straub JH, Klute S, Hunszinger V, Zech F, Prelli Bozzo C, Aftab W, Christensen MH, Conzelmann C, Müller JA, Srinivasachar Badarinarayan S, Stürzel CM, Forne I, Stenger S, Conzelmann K-K, Münch J, Schmidt FI, Sauter D, Imhof A, Kirchhoff F, and Sparrer KMJ**. Systematic functional analysis of SARS-CoV-2 proteins uncovers viral innate immune antagonists and remaining vulnerabilities. *Cell Reports* 35: 109126, 2021.

70. **Vazquez C, Swanson SE, Negatu SG, Dittmar M, Miller J, Ramage HR, Cherry S, and Jurado KA**. SARS-CoV-2 viral proteins NSP1 and NSP13 inhibit interferon activation through distinct mechanisms. *PLOS ONE* 16: e0253089, 2021.

bioRxiv preprint doi: https://doi.org/10.1101/2021.08.23.457411; this version posted August 25, 2021. The copyright holder for this preprint (which was not certified by peer review) is the author/funder. All rights reserved. No reuse allowed without permission.

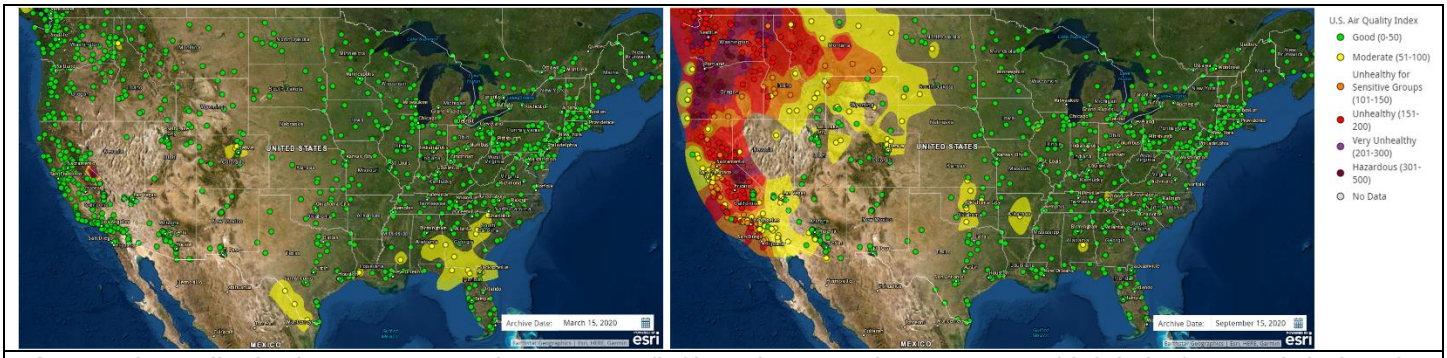

Fig. 1: Air quality in the US on March 15, 2020 (left) and September 15, 2020 (right), before and during the 2020 fire season, respectively. Air quality monitoring stations (dots) and contours report the daily air quality index as defined by the US Environmental Protection Agency based on PM2.5 and PM10. Images retrieved from AirNow (https://gispub.epa.gov/airnow/index.html?tab=3).

bioRxiv preprint doi: https://doi.org/10.1101/2021.08.23.457411; this version posted August 25, 2021. The copyright holder for this preprint (which was not certified by peer review) is the author/funder. All rights reserved. No reuse allowed without permission.

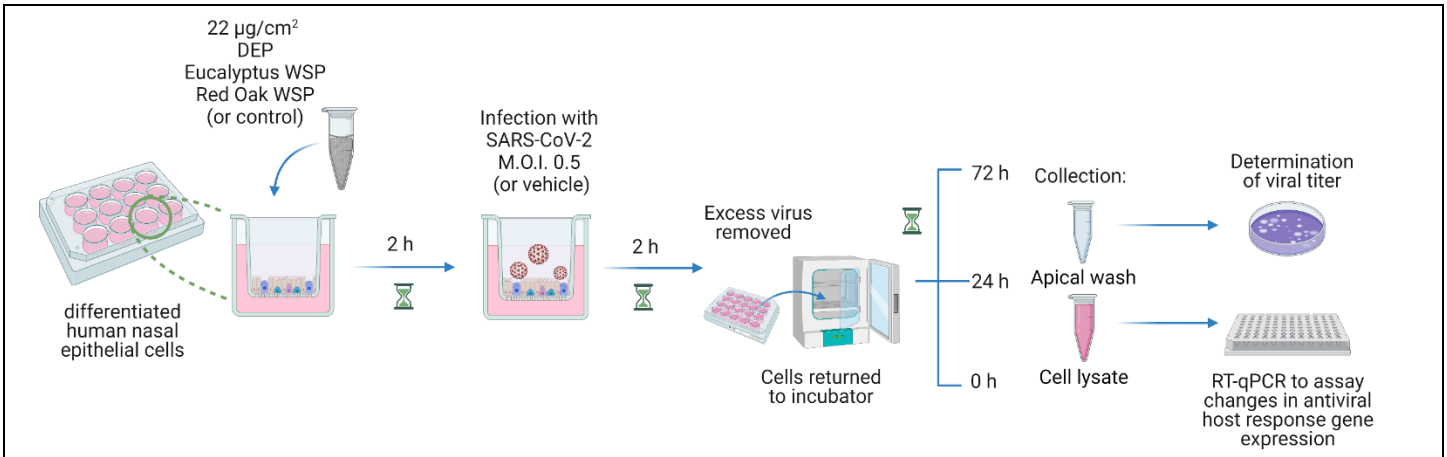

Fig. 2. Experimental design scheme. Differentiated hNECs from males and females grown at ALI were exposed to 22 µg/cm^2 DEP, eucalyptus WSP, or red oak WSP (or control) for 2 h. At the end of the exposure period, cells were infected with SARS-CoV-2 at an M.O.I. of 0.5 (or mock infected with vehicle) for 2 h. Excess virus/vehicle was then removed and the apical surface was washed. A second apical wash and cell lysis were performed immediately or 24 or 72 h later. Apical washes were used to determine viral titers and RNA was purified from cell lysates and used for RT-qPCR to assess altered gene expression in a panel of 48 genes. Figure created with BioRender.com.

bioRxiv preprint doi: https://doi.org/10.1101/2021.08.23.457411; this version posted August 25, 2021. The copyright holder for this preprint (which was not certified by peer review) is the author/funder. All rights reserved. No reuse allowed without permission.

Table 1: Demographic information about hNEC donors

	DEP (n=6)			Eucalyptus WSP (n=6)			Red Oak WSP (n=6)		
	Males (n=3)	Females (n=3)	**Aggregate (Males and Females)**	Males (n=3)	Females (n=3)	**Aggregate (Males and Females)**	Males (n=3)	Females (n=3)	**Aggregate (Males and Females)**
Age (mean ± SEM)	32±5.7	33.0±6.1	**32.5±3.7**	23.7±2.9	23.3±2.8	**23.5±1.8**	20.7±1.2	29.3±5.0	**25.0±3.0**
BMI (mean ± SEM)	27.8±3.1	26.5±1.4	**27.1±1.6**	23.5±0.8	29.9±6.1	**26.7±3.1**	24.3±1.5	26.9±3.8	**25.6±1.9**
Race: White/Black/Asian	2/1/0	3/0/0	**5/1/0**	1/0/2	2/1/0	**3/1/2**	0/0/3	1/1/1	**1/1/4**

bioRxiv preprint doi: https://doi.org/10.1101/2021.08.23.457411; this version posted August 25, 2021. The copyright holder for this preprint (which was not certified by peer review) is the author/funder. All rights reserved. No reuse allowed without permission.

Table 2: Genes assayed, grouped by functional categories. Assay identifiers are listed for TaqMan primer/probe sets purchased from Thermo Fisher (or IDT where indicated).

Gene Name:	Category:	TaqMan Probe Assay ID:
ACE2	Viral Entry Factor (VEF)	Hs01085331_m1
CTSB	Airway Proteases	Hs00157194_m1
CTSL		Hs00964651_m1
FURIN		Hs06637404_sH
MMP7		Hs01042796_m1
ST14		Hs01058386_m1
TMPRSS11D		Hs00975370_m1
TMPRSS2		Hs05024838_m1
IFIT1	Antiviral Defense	Hs03027069_s1
IFITM3		Hs03057129_s1
IFNA1		Hs04189288_g1
IFNA2		Hs00265051_s1
IFNB1		Hs00265051_s2
IFNG		Hs00265051_s3
IFNL1		Hs00265051_s4
IFNL2		Hs00265051_s5
LTF		Hs00265051_s6
MX1		Hs00265051_s7
SOCS3		Hs00265051_s8
CCL2	Cell Signaling/Immune Cell Recruitment	Hs00265051_s9
CCL3		Hs00265051_s10
CCL5		Hs00265051_s11
CSF2		Hs00265051_s12
CXCL10		Hs00265051_s13
CXCL11		Hs00265051_s14
CXCL8		Hs00265051_s15
CXCL9		Hs00265051_s16
IL15		Hs00265051_s17
IL1B		Hs00265051_s18
IL6		Hs00265051_s19
TNF		Hs00265051_s20
MUC5AC	Mucins	Hs00265051_s21
MUC5B		Hs00265051_s22
SFTPA1	Surfactant (Surf.)	Hs00265051_s23
SFTPD		Hs00265051_s24
IRF1	Transcription Factors	Hs00265051_s25
IRF3		Hs00265051_s26
IRF7		Hs00265051_s27
NFKB1		Hs00265051_s28
STAT1		Hs00265051_s29
STAT2		Hs00265051_s30
STAT3		Hs00265051_s31
DDX58	Viral Recognition	Hs00265051_s32
TLR3		Hs00265051_s33
TLR7		Hs00265051_s34
TLR9		Hs00265051_s35
nCoVN1	Viral Genes	IDT Cat # 10006713
nCoVN2		IDT Cat # 10006713
GAPDH	Reference Genes	Hs00265051_s36
ACTB		Hs00265051_s37
RP		IDT Cat # 10006713

bioRxiv preprint doi: https://doi.org/10.1101/2021.08.23.457411; this version posted August 25, 2021. The copyright holder for this preprint (which was not certified by peer review) is the author/funder. All rights reserved. No reuse allowed without permission.

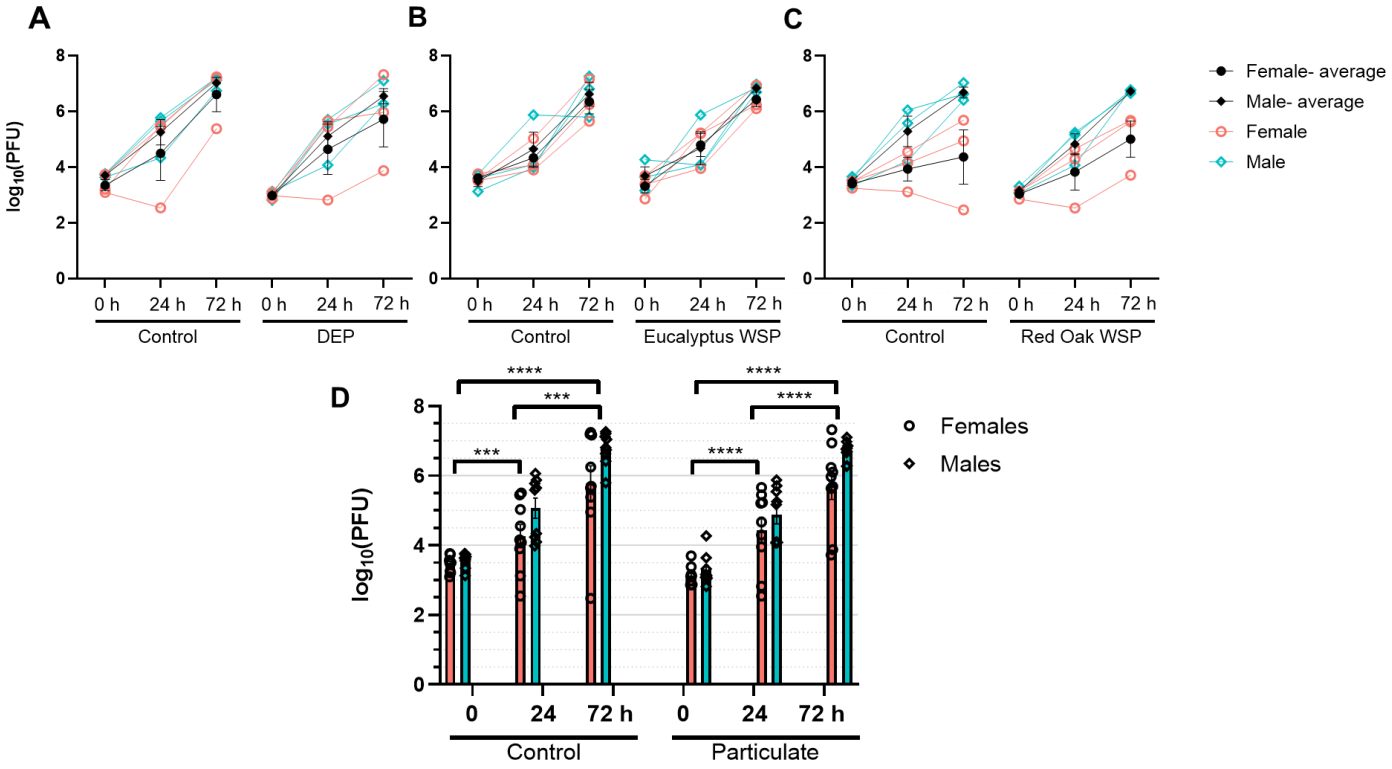

Fig. 3: SARS-CoV-2 viral titers in hNEC cultures at 0, 24, and 72 h p.i. hNECs from male and female donors were exposed to particulates (DEP or WSP from flaming eucalyptus or red oak, at 22 µg/cm^2) or control for 2 h, then infected with SARS-CoV-2 at an MOI of 0.5. At 0, 24, or 72 h post infection, the apical washes were collected and used for approximating viral titer. Titers from individual particulate exposures with respective controls for DEP, eucalyptus WSP, and red oak WSP are shown in **A-C** respectively. Black symbols indicate sex-specific means with standard error bars (N=3 biological replicates each for males and females). **D** Aggregated viral titers recovered from hNECs exposed to vehicle or a particulate. Standard error is shown (N=9 biological replicates for each bar). Unpaired t-tests with Welch's correction were used to determine (sex aggregated) differences in viral titer between time points, with *** p = 0.0001, **** p < 0.0001.

bioRxiv preprint doi: https://doi.org/10.1101/2021.08.23.457411; this version posted August 25, 2021. The copyright holder for this preprint (which was not certified by peer review) is the author/funder. All rights reserved. No reuse allowed without permission.

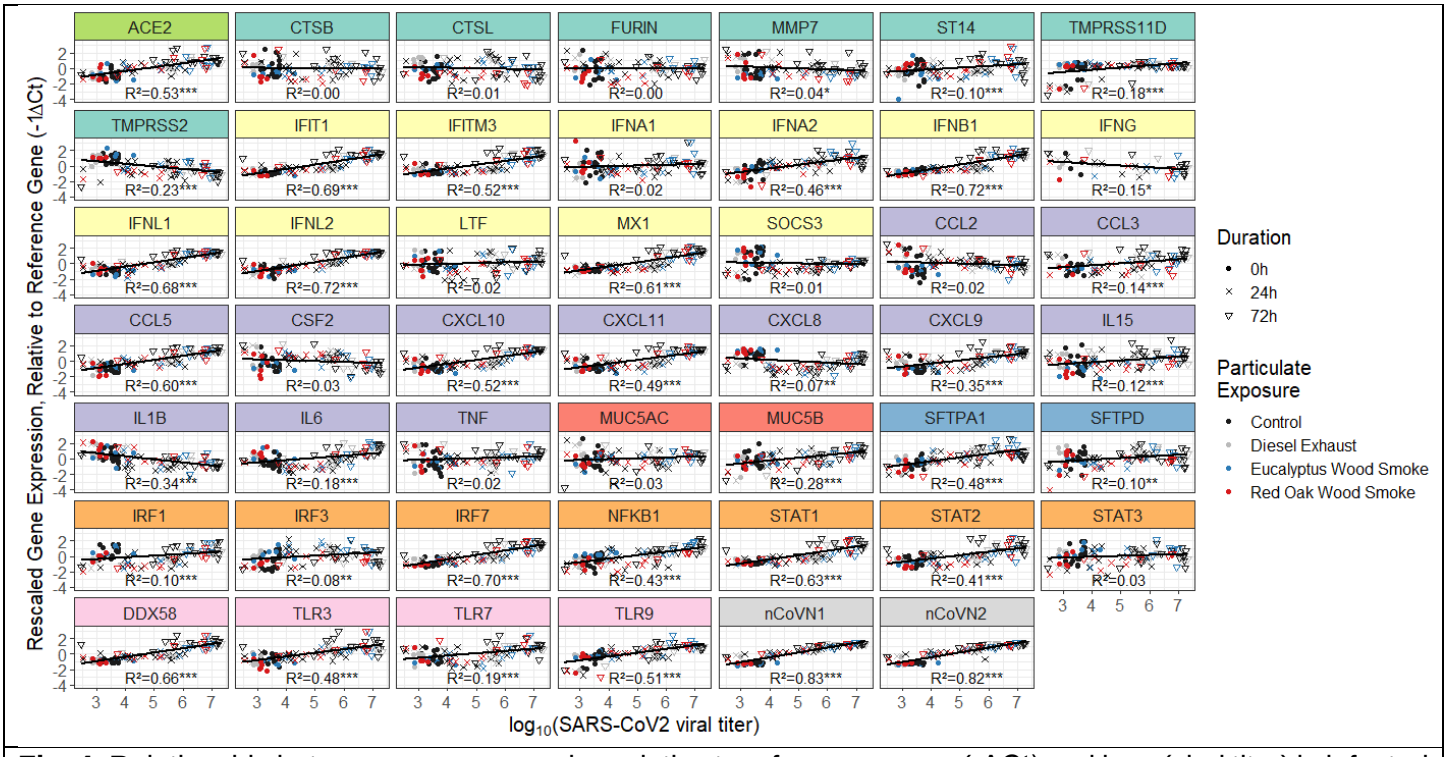

Fig. 4: Relationship between gene expression relative to reference genes (-ΔCt) and $\log_{10}$(viral titer) in infected cells. Colors behind gene names correspond to functional categories presented in Table 2. Statistical significance is indicated next to the coefficient of determination (R^2): * $p \leq 0.05$, ** $p \leq 0.01$, *** $p \leq 0.001$.

bioRxiv preprint doi: https://doi.org/10.1101/2021.08.23.457411; this version posted August 25, 2021. The copyright holder for this preprint (which was not certified by peer review) is the author/funder. All rights reserved. No reuse allowed without permission.

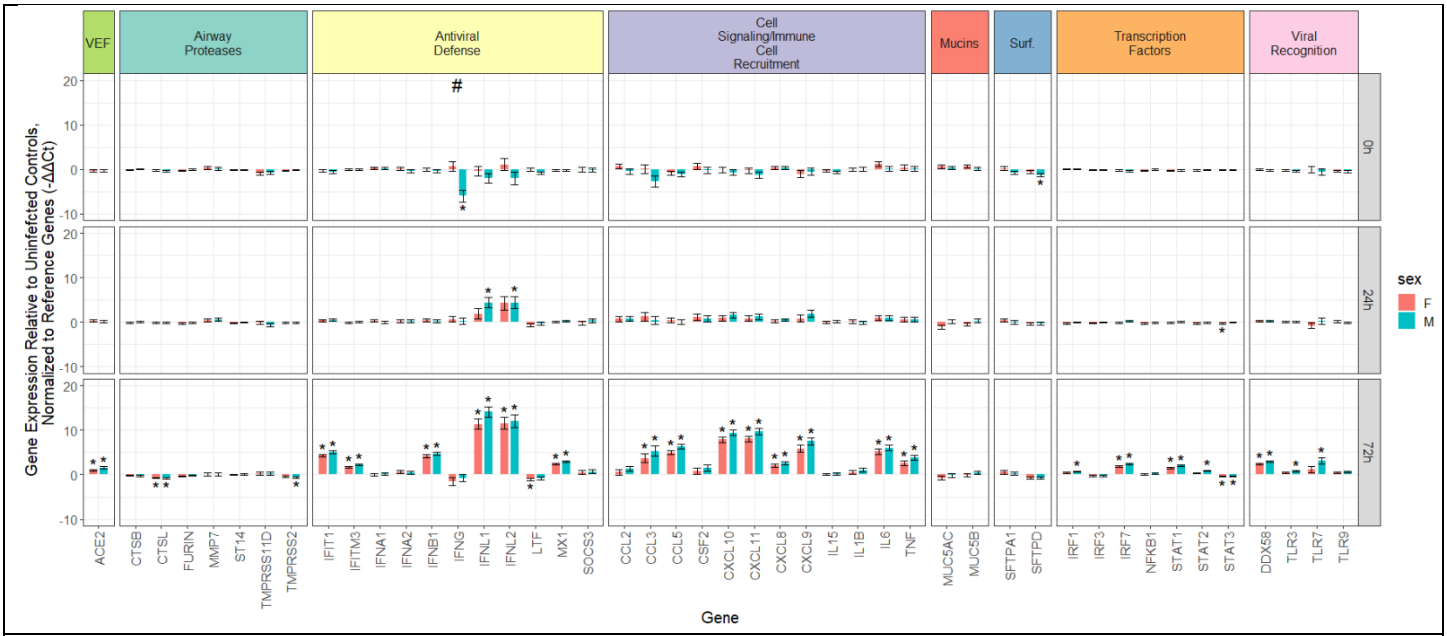

Fig. 5: Gene expression in infected hNECs from males and females relative to uninfected controls (-ΔΔCt) at 0, 24, and 72 h p.i. Gene categories are color-coded at the top, with 'VEF' an abbreviation for 'Viral Entry Factor' and 'Surf.' an abbreviation for 'Surfactant'. Graphed as average (N=9 biological replicates for each bar) with standard error. Statistically significant ($q \leq 0.05$) changes in gene expression are represented by *. A statistically significant difference in gene expression between males and females is indicated by #.

bioRxiv preprint doi: https://doi.org/10.1101/2021.08.23.457411; this version posted August 25, 2021. The copyright holder for this preprint (which was not certified by peer review) is the author/funder. All rights reserved. No reuse allowed without permission.

Table 3: Statistically significant virus-induced changes in gene expression in hNECs from males and females at 0, 24, and 72 h p.i. with SARS-CoV-2. N=9 biological replicates for individual sex effects (M or F) and N=18 for Combined effects.

Time	Gene	Sex	Fold induction	p-value
0 h	TMPRSS11D	Combined	0.583	0.002426089
	IFNG	Combined	0.159	0.003688264
	IFNG	M	0.016	9.74E-05
	IFNG	(#) M vs F	0.010	0.000409885
	SFTPD	Combined	0.538	9.32E-05
	SFTPD	M	0.417	9.81E-05
24 h	IFNL1	Combined	8.714	0.000145617
	IFNL1	M	20.685	0.000192167
	IFNL2	Combined	19.874	3.34E-05
	IFNL2	M	20.862	0.002065996
	STAT3	Combined	0.854	0.002007605
	STAT3	F	0.797	0.001628066
72 h	ACE2	Combined	2.423	<1.00E-15
	ACE2	M	3.004	5.50E-13
	ACE2	F	1.955	1.89E-06
	CTSL	Combined	0.592	1.69E-09
	CTSL	M	0.578	6.90E-06
	CTSL	F	0.605	1.98E-05
	TMPRSS2	Combined	0.681	1.11E-05
	TMPRSS2	M	0.646	0.000432043
	IFIT1	Combined	26.035	<1.00E-15
	IFIT1	M	34.117	<1.00E-15
	IFIT1	F	19.868	<1.00E-15
	IFITM3	Combined	3.904	<1.00E-15
	IFITM3	M	4.690	<1.00E-15
	IFITM3	F	3.251	<1.00E-15
	IFNB1	Combined	21.328	<1.00E-15
	IFNB1	M	25.399	<1.00E-15
	IFNB1	F	17.910	<1.00E-15
	IFNL1	Combined	6936.057	<1.00E-15
	IFNL1	M	17769.309	<1.00E-15
	IFNL1	F	2707.414	<1.00E-15
	IFNL2	Combined	3694.082	<1.00E-15
	IFNL2	M	4439.865	3.20E-14
	IFNL2	F	3073.571	1.60E-14
	LTF	Combined	0.532	0.000174964
	LTF	F	0.481	0.001623359
	MX1	Combined	6.403	<1.00E-15
	MX1	M	7.953	<1.00E-15
	MX1	F	5.156	<1.00E-15
	CCL3	Combined	23.013	1.00E-07
	CCL3	M	39.806	2.81E-05
	CCL3	F	13.305	0.000310249

bioRxiv preprint doi: https://doi.org/10.1101/2021.08.23.457411; this version posted August 25, 2021. The copyright holder for this preprint (which was not certified by peer review) is the author/funder. All rights reserved. No reuse allowed without permission.

	CCL5	Combined	50.332	<1.00E-15
	CCL5	M	80.165	<1.00E-15
	CCL5	F	31.601	<1.00E-15
	CXCL10	Combined	407.908	<1.00E-15
	CXCL10	M	690.693	<1.00E-15
	CXCL10	F	240.902	<1.00E-15
	CXCL11	Combined	466.263	<1.00E-15
	CXCL11	M	830.134	<1.00E-15
	CXCL11	F	261.905	<1.00E-15
	CXCL8	Combined	4.983	<1.00E-15
	CXCL8	M	5.969	8.79E-12
	CXCL8	F	4.160	9.03E-09
	CXCL9	Combined	101.793	<1.00E-15
	CXCL9	M	180.869	<1.00E-15
	CXCL9	F	57.290	2.53E-11
	IL6	Combined	48.590	<1.00E-15
	IL6	M	65.435	<1.00E-15
	IL6	F	36.082	<1.00E-15
	TNF	Combined	9.221	6.90E-14
	TNF	M	14.853	8.81E-11
	TNF	F	5.724	7.13E-06
	SFTPD	Combined	0.600	0.001390553
	IRF1	Combined	1.487	3.15E-07
	IRF1	M	1.648	6.01E-06
	IRF3	Combined	0.829	0.001101794
	IRF7	Combined	4.506	<1.00E-15
	IRF7	M	5.342	<1.00E-15
	IRF7	F	3.800	<1.00E-15
	STAT1	Combined	3.400	<1.00E-15
	STAT1	M	4.004	<1.00E-15
	STAT1	F	2.887	<1.00E-15
	STAT2	Combined	1.541	1.03E-07
	STAT2	M	1.854	1.23E-07
	STAT3	Combined	0.760	2.63E-07
	STAT3	M	0.765	0.000335234
	STAT3	F	0.756	0.000116706
	DDX58	Combined	6.407	<1.00E-15
	DDX58	M	7.883	<1.00E-15
	DDX58	F	5.207	<1.00E-15
	TLR3	Combined	1.488	1.30E-05
	TLR3	M	1.666	8.77E-05
	TLR7	Combined	4.575	1.36E-05
	TLR7	M	9.119	1.06E-05
	TLR9	Combined	1.469	0.000994151

bioRxiv preprint doi: https://doi.org/10.1101/2021.08.23.457411; this version posted August 25, 2021. The copyright holder for this preprint (which was not certified by peer review) is the author/funder. All rights reserved. No reuse allowed without permission.

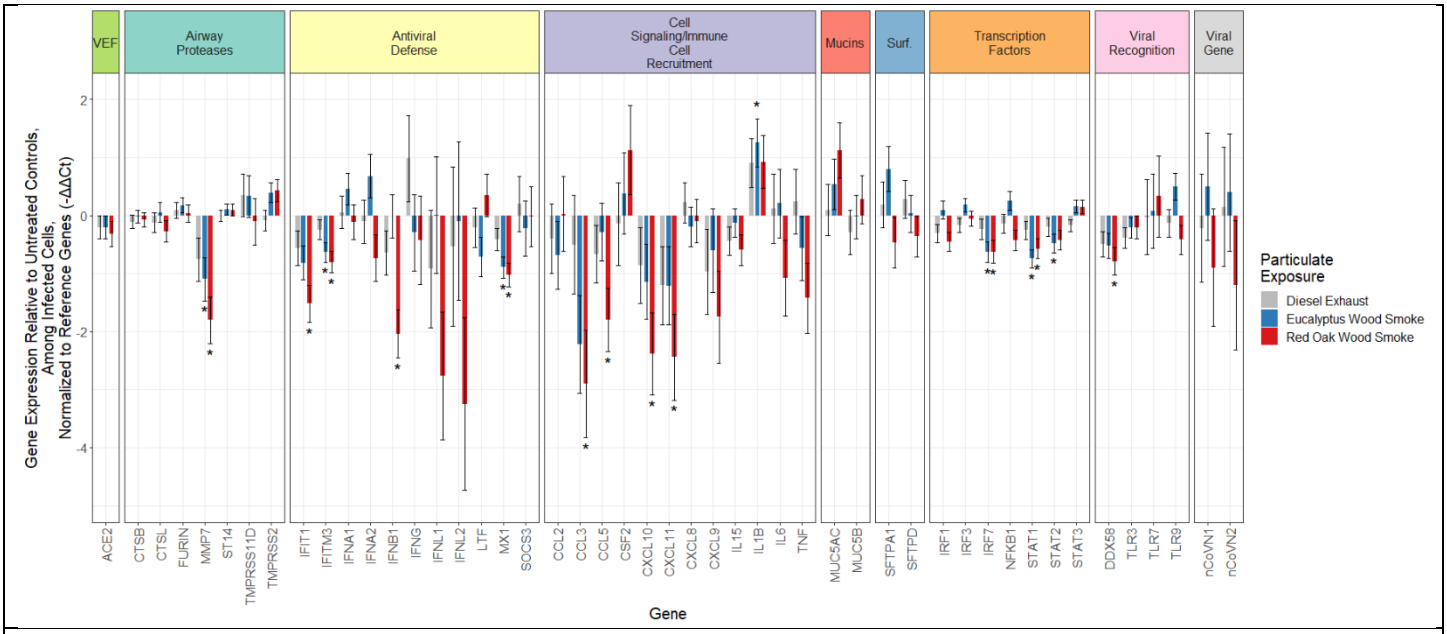

Fig. 6: Effects of particulate exposure (DEP and WSP) on virus-induced gene expression in infected hNECs at 72 h p.i. Graphed as means with black bars representing standard error. Males and females are combined for N=6 biological replicates per bar. Statistically significant changes in gene expression are indicated by * ($q \leq 0.05$).

bioRxiv preprint doi: https://doi.org/10.1101/2021.08.23.457411; this version posted August 25, 2021. The copyright holder for this preprint (which was not certified by peer review) is the author/funder. All rights reserved. No reuse allowed without permission.

Table 4. Statistically significant effects of particulate exposure on virus-induced gene expression in hNECs at 0, 24, and 72 h p.i. N=6 (3M, 3F) biological replicates per measurement.

Time	Gene	Particulate	Sex	Fold induction	p-value
0 h	IRF1	DEP	Combined	0.638	3.60725E-05
	IL1B	Eucalyptus WSP	Combined	2.553	0.001377971
	IL6	Eucalyptus WSP	Combined	4.024	7.84E-04
	CTSB	Red Oak WSP	Combined	0.780	0.001893867
	IL1B	Red Oak WSP	Combined	2.496	1.97E-03
	IL6	Red Oak WSP	Combined	8.519	5.59E-07
	STAT2	Red Oak WSP	Combined	0.722	0.003403266
24 h	IL1B	DEP	Combined	3.530	2.77506E-05
	IL1B	Eucalyptus WSP	Combined	3.691	1.13E-05
	CTSB	Red Oak WSP	Combined	0.736	0.000145452
	FURIN	Red Oak WSP	Combined	0.708	0.00023035
	MMP7	Red Oak WSP	Combined	0.413	0.000723912
	MX1	Red Oak WSP	Combined	0.663	1.68E-03
	IL1B	Red Oak WSP	Combined	3.299	6.47E-05
	STAT2	Red Oak WSP	Combined	0.690	8.85E-04
72 h	MMP7	Eucalyptus WSP	Combined	0.467	3.38E-03
	IFITM3	Eucalyptus WSP	Combined	0.644	2.08E-04
	MX1	Eucalyptus WSP	Combined	0.539	3.55E-06
	IL1B	Eucalyptus WSP	Combined	2.385	3.20E-03
	IRF7	Eucalyptus WSP	Combined	0.647	6.52E-04
	STAT1	Eucalyptus WSP	Combined	0.597	4.38E-06
	STAT2	Eucalyptus WSP	Combined	0.717	2.85E-03
	MMP7	Red Oak WSP	Combined	0.286	1.64556E-05
	IFIT1	Red Oak WSP	Combined	0.349	5.96E-06
	IFITM3	Red Oak WSP	Combined	0.572	2.03E-05
	IFNB1	Red Oak WSP	Combined	0.243	2.10E-06
	MX1	Red Oak WSP	Combined	0.493	1.46E-06
	CCL3	Red Oak WSP	Combined	0.134	2.30E-03
	CCL5	Red Oak WSP	Combined	0.287	1.15E-03
	CXCL10	Red Oak WSP	Combined	0.192	9.47E-04
	CXCL11	Red Oak WSP	Combined	0.184	1.13E-03
	IRF7	Red Oak WSP	Combined	0.647	1.90E-03
	STAT1	Red Oak WSP	Combined	0.673	1.07E-03
	DDX58	Red Oak WSP	Combined	0.578	1.08E-03

bioRxiv preprint doi: https://doi.org/10.1101/2021.08.23.457411; this version posted August 25, 2021. The copyright holder for this preprint (which was not certified by peer review) is the author/funder. All rights reserved. No reuse allowed without permission.

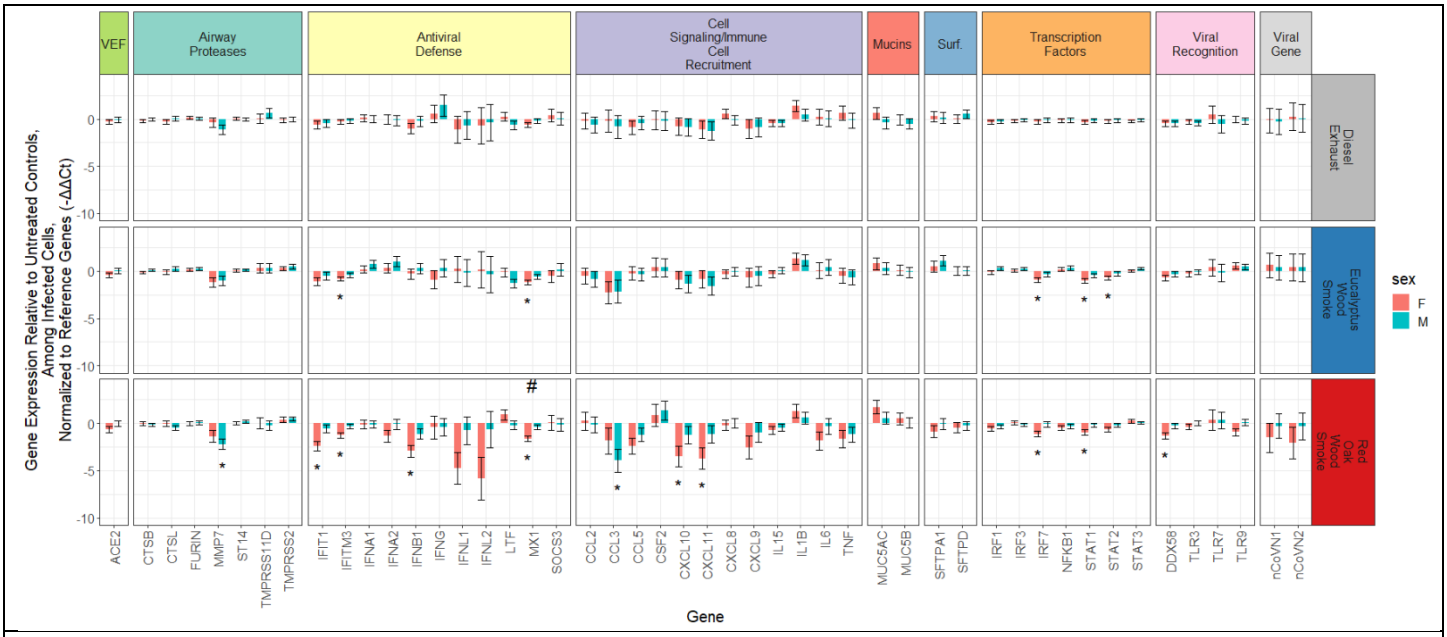

Fig. 7: Effects of particulate exposure on virus-induced gene expression in infected hNECs from males or females at 72 h post infection. Graphed as means with black bars representing standard error, N=3 biological replicates per bar. Statistically significant changes in gene expression are represented by * and statistically significant differences in expression between males and females are represented by # ($q \leq 0.05$).

bioRxiv preprint doi: https://doi.org/10.1101/2021.08.23.457411; this version posted August 25, 2021. The copyright holder for this preprint (which was not certified by peer review) is the author/funder. All rights reserved. No reuse allowed without permission.

Table 5. Statistically significant, sex-disaggregated effects of particulate exposure on virus-induced gene expression in infected hNECs at 0, 24, and 72 h p.i. N=3 biological replicates per measurement.

Time	Gene	Particulate	Sex	Fold induction	p-value
0 h	IRF1	DEP	M	0.586	0.00046212
	IL6	Red Oak WSP	M	8.773	0.000240913
	IL6	Red Oak WSP	F	8.271	3.87E-04
	TLR3	Red Oak WSP	M	0.580	0.002197364
24 h	IL1B	DEP	M	4.956	1.57E-04
	IL1B	Eucalyptus WSP	F	4.695	2.17E-04
	FURIN	Red Oak WSP	F	0.665	0.002092396
	IL1B	Red Oak WSP	F	3.398	0.003538543
72 h	IFITM3	Eucalyptus WSP	F	0.565	5.88E-04
	MX1	Eucalyptus WSP	F	0.434	8.25069E-06
	IRF7	Eucalyptus WSP	F	0.524	0.000329325
	STAT1	Eucalyptus WSP	F	0.493	7.24008E-06
	STAT2	Eucalyptus WSP	F	0.615	1.97E-03
	MMP7	Red Oak WSP	M	0.215	4.72E-05
	IFIT1	Red Oak WSP	F	0.184	1.63E-06
	IFITM3	Red Oak WSP	F	0.413	9.25E-06
	IFNB1	Red Oak WSP	F	0.130	6.06E-06
	MX1	Red Oak WSP	F	0.322	3.90E-07
	MX1	Red Oak WSP	(#) M vs F	2.347	2.96E-03
	CCL3	Red Oak WSP	M	0.065	1.60E-03
	CXCL10	Red Oak WSP	F	0.089	1.35E-03
	CXCL11	Red Oak WSP	F	0.076	1.05E-03
	IRF7	Red Oak WSP	F	0.452	0.000198042
	STAT1	Red Oak WSP	F	0.516	3.37E-04
	DDX58	Red Oak WSP	F	0.403	3.60E-04